Evidence of intrinsic ferromagnetism in individual dilute magnetic semiconducting nanostructures

Z. H. Zhang[1,5], Xuefeng Wang[2,6], J. B. Xu[2], S. Muller[3], C. Ronning[4] and Quan Li[1]*

Semiconductors doped with magnetic ions, also known as dilute magnetic semiconductors, are both semiconducting and ferromagnetic. It remains unclear, however, whether this ferromagnetism is intrinsic, as is required for spintronic applications, or is due instead to dopant clustering. Here, we report conclusive evidence for intrinsic ferromagnetism in individual ZnO nanoparticles doped with transition metal ions. Through a simultaneous magnetic and microstructural characterization using electron magnetic chiral dichroism and channelling-enhanced electron energy loss microanalysis, respectively, we show that ZnO nanoparticles have intrinsic ferromagnetism when doped with cobalt, but not when doped with iron.

The observation of ferromagnetism in dilute magnetic semiconductors (DMS) has led to intense research interest in these materials due to their potential for use in spintronic devices, which make use of both the spin and charge of electrons[1]. Practical applications of DMS materials would require both a Curie temperature above room temperature and a ferromagnetism that is intrinsic, rather than one due to the presence of magnetic clusters of dopants. These requirements make transition-metal-doped ZnO a particularly promising system due to the observation of room-temperature ferromagnetism in several different ZnO-based systems including manganese- and cobalt-doped ZnO (refs 2–4).

Although a large number of studies on transition-metal-doped ZnO are available in the literature, many are in conflict with one another. More importantly, there is no consensus on whether the observed ferromagnetism is intrinsic. Most measurements provide experimental evidence that is only indicative of, rather than exclusive to, intrinsic ferromagnetism[5,6]. The anomalous Hall effect[7,8] had been regarded as a piece of direct evidence for intrinsic ferromagnetism in DMS, but was found to be inadequate when such an effect was also observed in non-ferromagnetic specimens[9,10].

Generally speaking, the possible existence of magnetic clusters in ZnO is almost impossible to exclude on the basis of macroscopic measurement data. On the other hand, it is also difficult when microscopic solutions are sought, because the evaluation of the magnetic properties of individual nano-objects, simultaneous with structural characterization, has not been available. This is particularly troublesome in nanostructured ZnO systems owing to the non-uniform characteristic of the nano-samples. Consequently, establishment of a clear and direct connection between microstructure and magnetic behaviour for individual ZnO nanostructures (doped with a transition metal) has been absent so far, and claims of intrinsic ferromagnetism in these materials cannot be definitive without such characterization.

In the present work we have tackled the above-mentioned problem by analysing a single-doped ZnO nanostructure in a transmission electron microscope (TEM). The dopant sites (interstitial versus substitutional) in the ZnO matrix have been determined using atom location by channelling-enhanced microanalysis (ALCHEMI), and the magnetic properties of the same individual nanostructures have been deduced from electron magnetic chiral dichroism (EMCD) measurements. ZnO nanoparticles doped with two different transition metal ions (cobalt and iron) were chosen as examples to illustrate such an investigation. Taking advantage of the excellent spatial resolution in a TEM, the combination of these two microscopic techniques allows the simultaneous assessment of both microstructure and magnetic behaviour of the individual nanostructures. Despite the structural similarities between the cobalt- and iron-doped ZnO nanoparticles, their magnetic behaviours are found to be different.

Microstructures of the doped ZnO nanoparticles

Typical morphologies of the cobalt- and iron-doped ZnO nanoparticles are shown in Fig. 1a and b, respectively. Selected area electron diffraction patterns taken from individual nanoparticles (from both cobalt- and iron-doped samples) reveal their single crystalline hexagonal structure, which is further confirmed by the corresponding high-resolution images shown in Fig. 1c and d, respectively. Few defects of either line or plane type are observed in the ZnO lattice. The local chemical compositions of the samples were characterized by energy dispersive X-ray spectroscopy (EDS) using a ~1-nm electron probe. Figure 1e shows the existence of zinc, oxygen and cobalt in the cobalt-doped ZnO nanoparticles, and Fig. 1f shows zinc, oxygen and iron in the iron-doped ZnO nanoparticles. In each of the samples, EDS was performed at several different locations in the same nanoparticle, resulting in the identification of similar chemical compositions, which suggests a fairly uniform distribution of the dopant ions. No clustering of the cobalt or iron was observed, and their concentrations were estimated at ~5.6% and ~4%, respectively.

Dopant sites in the ZnO lattice

Although obvious clustering/phase separation can be excluded from the TEM imaging, it is still necessary to determine the sites of the dopants in the ZnO lattice. If the transition metal ions are to occupy the interstitial sites, their possibly non-uniform distribution could lead to locally high concentrations of the ions in the ZnO (although

[1]Department of Physics, The Chinese University of Hong Kong, Shatin, New Territory, Hong Kong SAR, China, [2]Department of Electronic Engineering and Materials Science and Technology Research Center, The Chinese University of Hong Kong, Shatin, New Territory, Hong Kong SAR, China, [3]Institute of Physics, University of Gottingen, Friedrich-Hund-Platz 1, 37077 Gottingen, Germany, [4]Institute of Solid State Physics, University of Jena, Max-Wien-Platz 1, 07743 Jena, Germany, [5]Liaoning Key Materials Laboratory for Railway, DaLian JiaoTong University, DaLian, China, [6]Department of Physics, Soochow University, Suzhou 215006, China. *e-mail: liquan@phy.cuhk.edu.hk
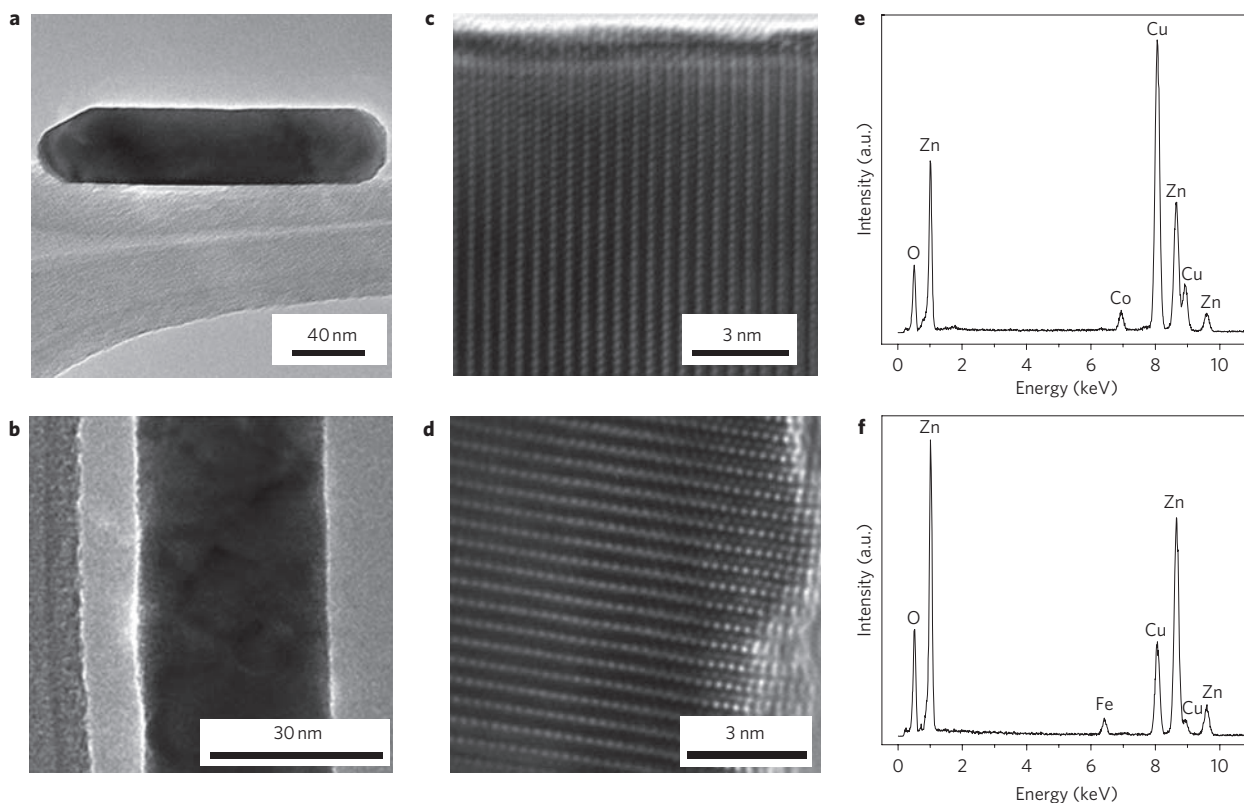
Figure 1 | TEM images and EDS results taken from the cobalt- and iron-doped ZnO samples, disclosing their morphologies, microstructures and chemical compositions. a,b, Low-magnification TEM images of the cobalt-doped (**a**) and iron-doped (**b**) ZnO samples. **c,d,** High-resolution TEM image taken at the surface region for the cobalt-doped (**c**) and iron-doped (**d**) ZnO samples. **e,f,** Typical EDS results obtained from cobalt-doped (**e**) and iron-doped (**f**) ZnO sample. The cobalt and iron concentrations in the samples are ∼5.6% and ∼4%, respectively.

chemical bonding among the transition metal ions and thus a second phase in the format of metal clusters has not formed). Such local enrichment may lead to specific magnetic behaviour of the doped compound, but the magnetic behaviour would originate from the direct interaction of the transition metal ions due to their small separation distance rather than fitting into the general picture of DMS[11,12]. In the present study, the type of dopant site(s) in the ZnO lattice was determined by ALCHEMI–electron energy loss spectroscopy (EELS)[13–15]. This method can differentiate the substitutional sites from the interstitial ones, and a comparable resolution is not achievable using other techniques such as X-ray photoelectron spectroscopy[16].

Figure 2 plots the normalized peak intensities (with respect to that of oxygen) of zinc and cobalt (or iron) as a function of the orientation parameter $\Delta\theta$, based on ALCHEMI–EELS spectra (see Supplementary Fig. S1) taken from the cobalt- and iron-doped ZnO samples. When considering the case of pure ZnO, the EELS core loss ionization edge intensity of zinc and oxygen would change in an opposite manner as $\Delta\theta$ varies from –1.8 to 1.8 mrad, as determined by the non-centrosymmetrical nature of the lattice[15]. In the present study, for both the cobalt- (Fig. 2a) and iron-doped ZnO (Fig. 2b) samples, the trend of the zinc ionization edge intensity change as a function of $\Delta\theta$ was found to be similar to that of the transition metal dopants, suggesting that the dopants take the substitutional sites of the zinc in the ZnO lattice.

Intrinsic magnetism of the doped nanoparticles

EMCD measurements were performed on the same nanostructure to characterize the magnetic behaviour. The feasibility of EMCD measurements was first proposed in 2003 (ref. 17) and was experimentally demonstrated in 2006 in a single-crystalline iron thin film epitaxially grown on a GaAs substrate[18]. The equivalence of the

momentum transfer **q** in EELS to the linear polarization vector **ε** in X-ray absorption spectroscopy[19] allows the magnetic circular dichroism to be measured in the absence of a spin-polarized electron beam. Two requirements must be satisfied to enable the EMCD measurement. First, two chiral positions for spectra acquisition must be generated. This can be achieved by tilting the specimen to a two-beam condition, as illustrated by the inset in Fig. 3a. The '+' and '−' positions in the diffraction pattern are lined up with mirror symmetry with respect to the **g** reciprocal lattice vector. They are equivalent to the result generated by the left and right circular light in X-ray magnetic circular dichroism[19]. The EELS results acquired at '+' and '−' thus correspond to opposite chirality conditions due to the opposite sign of momentum transfer (**q**) at the '+' and '−' positions, respectively. Second, the magnetization of the specimen must have its net magnetic moment aligned in a direction parallel/antiparallel to the incident electron beam to achieve a maximum dichroism[19]. Initial magnetization of the samples can be achieved easily with the TEM objective lens pole piece, which gives a magnetic field of ∼2 T that is large enough to saturate the ZnO-based DMS materials[16].

The Co (Fe)-$L_{2,3}$ edge spectra were collected at both '+' and '−' positions, and the difference spectra that give the dichroic signals were calculated by subtracting the corresponding '+' spectra from the '−' spectra. The data shown in Fig. 3 were obtained with the objective lens on. For both cobalt- and iron-doped ZnO samples, the intensity of the transition metal L_3 edge taken at the '+' position is higher than that taken at the '−' position the opposite is true for the case of the L_2 edge. Consequently, non-zero difference spectra always result from both samples.

The origin of the dichroic signals at the $L_{2,3}$ edges of the transition metal ions can be illustrated as follows. The L_3 and L_2 edges in the core-loss EELS originate from the spin–orbit split
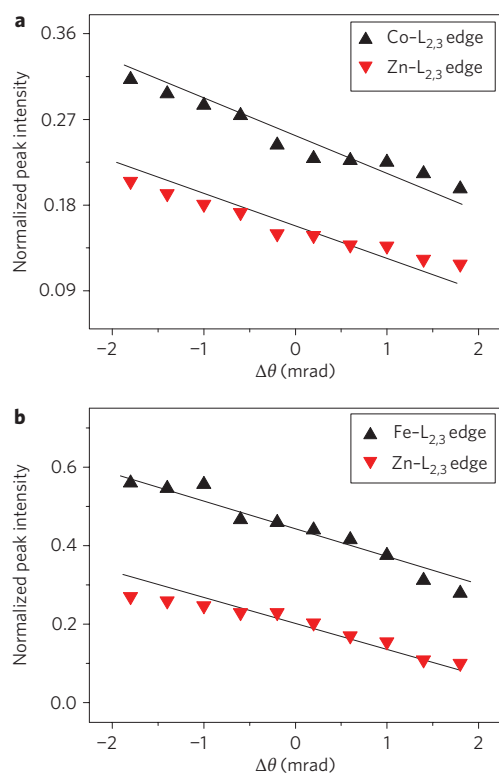
Figure 2 | Dependence of the normalized peak intensities (with respect to that of the O-K edge) of the Zn-L$_{2,3}$ edge, the Co-L$_{2,3}$ edge and the Fe-L$_{2,3}$ edge on the orientation parameter ($\Delta\theta$). Normalized peak intensities of the Zn-L$_{2,3}$ edge and the Co-L$_{2,3}$ edge (**a**) and the Zn-L$_{2,3}$ edge and the Fe-L$_{2,3}$ edge (**b**) as a function of $\Delta\theta$ in cobalt-doped and iron-doped ZnO samples, respectively. The cobalt and iron concentrations in the samples are ~5.6% and ~4%, respectively.

p-states to the unoccupied $3d$ states (splitting into spin-up and spin-down bands) in the conduction band[20]. The interaction of the incident electrons with the p-electrons (in the material) for opposite chirality conditions (corresponding to '+' and '−' positions) leads to the excitation of spin-polarized electrons. At the '−' position, fewer spin-up electrons and more spin-down electrons are excited, the opposite results being obtained at the '+' position. Consequently, in a non-magnetic material, one should not expect any difference in the L$_3$(L$_2$) edge intensity for spectra taken at the '+' and '−' positions. As soon as there is an imbalance in the number of available empty spin-up and -down states, the absorption at the two polarizations ('+' and '−' positions) will be different, and such a difference is exactly the opposite for the L$_3$ and L$_2$ edges. Therefore, comparison of the intensity changes of both L$_3$ and L$_2$ edges at the '+' and '−' positions (the dichroism spectra shown in Fig. 3) will mainly describe the difference between the spin populations. As the magnetic properties of the transition metals are mainly determined by the spin imbalance of $3d$ electrons, information on the difference in intensity of the L$_3$ and L$_2$ edges would thus provide a direct evaluation of the magnetic behaviour of the material. Consequently, the EMCD measurement on the transition metal dopants in the ZnO would provide information on the difference in the spin populations of the doped compounds, and their magnetic properties can be deduced accordingly.

The possible contributions to the difference in the spin populations of the transition-metal-doped ZnO are now considered. Note that room-temperature ferromagnetism has been observed in cobalt-doped ZnO[16], but iron-doped ZnO exhibits paramagnetism at room temperature, as suggested by superconducting quantum
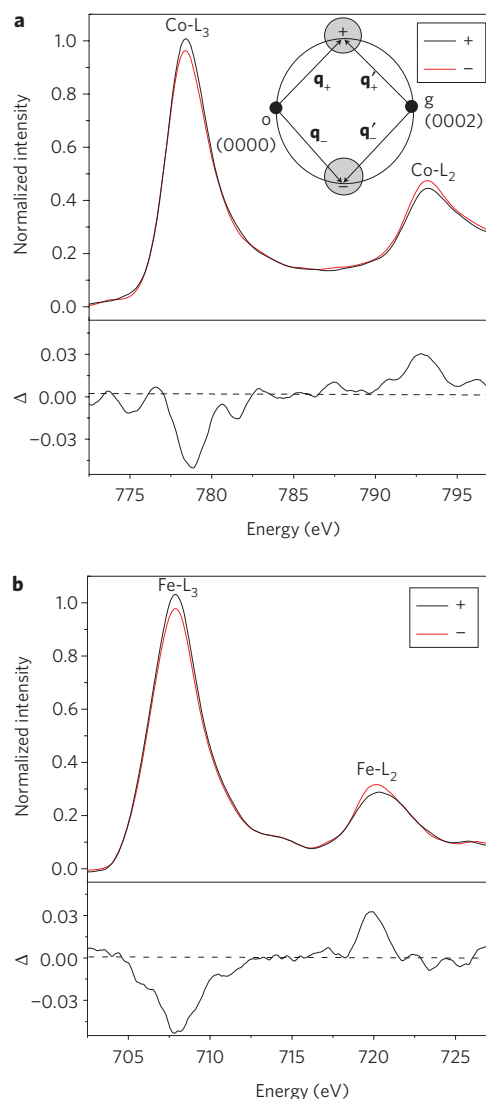
Figure 3 | Typical EMCD results for the cobalt- and iron-doped ZnO samples obtained under the objective lens. a, The Co-L$_{2,3}$ edges taken from two chiral positions '+' and '−', as indicated by the inset, and the difference spectrum, disclosing the spin population difference. The '+' and '−' position correspond to the superposition of two groups of momentum transfer vector ($\mathbf{q}_+$, $\mathbf{q}'_+$ and $\mathbf{q}_-$, $\mathbf{q}'_-$), with $|\mathbf{q}| = |\mathbf{q}'|$ and an angle of $\pi/2$ between $\mathbf{q}$ and $\mathbf{q}'$. In the inset, 'o' and 'g' represent the transmitted spot (0000) and the (0002) diffraction spot in the diffraction pattern, respectively. **b,** The Fe-L$_{2,3}$ edges taken from the two chiral positions, '+' and '−', and the difference spectrum.

interference device (SQUID) magnetometric measurement performed at the macroscopic scale (see Supplementary Figs S2 and S3). Consequently, although the non-zero difference spectra indeed reveal a difference between the spin populations of the iron or cobalt sub-lattices for both cobalt- and iron-doped samples, they must be of different origins. In the cobalt-doped ZnO, both a spin split impurity band and unpaired electrons of the $3d$ ions (see Fig. 4a) contribute to the spin imbalance in the empty density of states (DOS) and consequently the final magnetic behaviour of the material[11,12]. However, in the paramagnetic iron-doped ZnO, the spin-polarized DOS only change from symmetric (Fig. 4b) to asymmetric (for spin-up and spin-down electrons) when the external magnetic field is applied[21]. Therefore, the observed difference in the spin populations in the above EMCD experiments at fixed large magnetic field (with objective lens on),
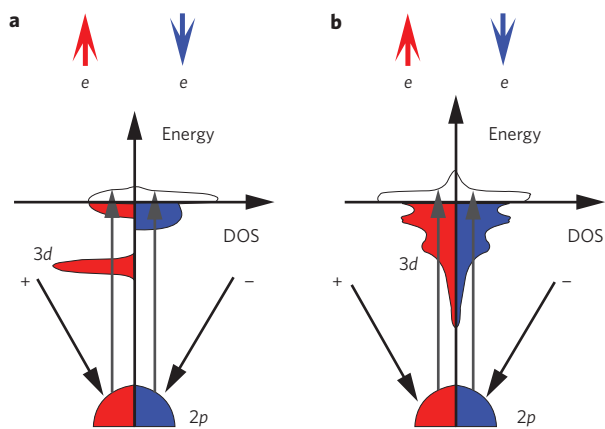
Figure 4 | Schematic of the density of states (DOS) of the cobalt- and iron-doped ZnO samples. a, The projected DOS of the cobalt-doped ZnO. The initial $2p$ electrons with different spin configurations (up and down) are excited to the spin-polarized empty DOS. The spin imbalance of the empty DOS accounts for the observed dichroism. **b,** The total DOS of the iron-doped ZnO in the absence of an external field. The symmetrical characteristic indicates the absence of dichroism for iron-doped ZnO when the external field is removed. In both **a** and **b**, the tilted arrows (black) represent the preferred momentum transfer at different chiral ('+' and '−') positions. The straight arrows (grey) represent the excitation direction, the red and blue colours represent the 'spin-up' and 'spin-down' occupied DOS, respectively, and the white colour represents the empty DOS.

together with the identification of the dopant sites (substitutional and no clusters), only confirms intrinsic magnetism in both samples, but not necessarily intrinsic ferromagnetism.

Intrinsic ferromagnetism of the cobalt-doped ZnO

The same EMCD experiments were carried out, but with a Lorentz lens, which exerts a very low magnetic field (∼17 Oe in the present study) on the specimen. The corresponding data are shown in Fig. 5, in which distinctly different results are observed for the cobalt- and iron-doped ZnO nanoparticles. A chiral dichroism signal is observed for the Co-$L_{2,3}$ edges, but not the Fe-$L_{2,3}$ edges. Such results therefore give unambiguous evidence of spontaneous magnetic ordering in the absence of an external field, and thus indicate intrinsic ferromagnetism in the cobalt-doped ZnO sample only. For the cobalt-doped ZnO sample, it should also be noted that there is a difference in the macroscopic (SQUID measurement) and microscopic (EMCD) data. In the SQUID measurement, the magnetic moment of the whole nanoparticle sample results from the summation of all individual domains. However, in the EMCD measurement, only a local area of a single nanoparticle is probed, with the dichroism signal representing the magnetization of the local region. Consequently, one would expect a possible intensity variation in the dichroism signals of the cobalt-doped ZnO nanoparticles being probed, as has indeed been observed in examinations of tens of particles (see example in Supplementary Fig. S6).

Conclusion

A combination of ALCHEMI–EELS and EMCD measurements performed in a TEM enables the direct evaluation on the intrinsic magnetism of individual ZnO nanostructures doped with transition metal ions. Our experimental results give unambiguous evidence for intrinsic ferromagnetism in cobalt-doped ZnO nanoparticles, clarifying the long-term argument on the magnetic properties of the material. The excellent spatial resolutions of the techniques make it possible to simultaneously evaluate the microstructure and magnetism of an individual nano-sample, thus allowing direct correlation to be locally established. This eliminates the ambiguity
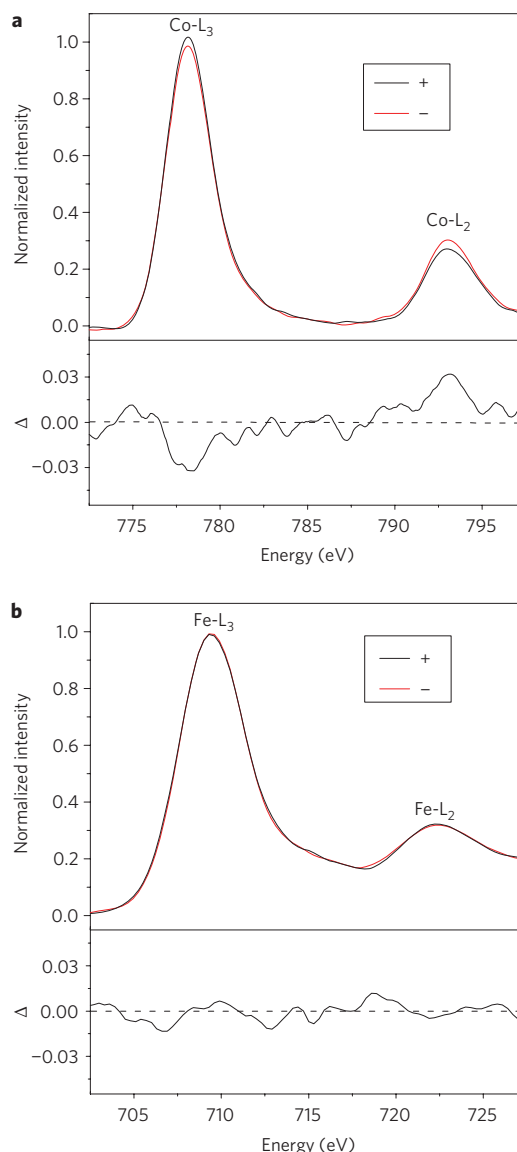
Figure 5 | EMCD results and the corresponding difference spectra of the cobalt- and iron-doped ZnO samples obtained under the Lorentz lens. a,b, The Co-$L_{2,3}$ edges (**a**) and the Fe-$L_{2,3}$ edges (**b**) taken from the two chiral positions '+' and '−'.

commonly associated with all macroscopic characterization techniques ubiquitously used for DMS materials. Such techniques can be applied to a variety of transition-metal-doped semiconductor material systems and serve as a direct justification for their possible intrinsic ferromagnetism, paving the way for their future applications in spintronic devices.

Methods

The studied cobalt-doped ZnO nanoparticles were synthesized using a simple solvothermal technique[16], and the samples demonstrated a robust room-temperature ferromagnetic behaviour for measurements carried out at a macroscopic scale. The sample with a cobalt concentration of ∼5.6% was chosen for the EELS measurement, as this had the largest saturation magnetic moments of all the doped samples and thus had the best signal-to-noise ratio in the EELS measurements. The iron-doped ZnO nanowires with an iron concentration of ∼4% were obtained by ion implantation of ZnO nanowires synthesized by thermal evaporation[22]. The macroscopic magnetic properties of the samples were measured using a Quantum Design SQUID magnetometer. The microstructures of the samples were examined using various TEM-related techniques (Tecnai F20 ST, operating at 200 kV). The EELS experiments, including both the ALCHEMI and EMCD measurements, were performed using a post-column Gatan Imaging Filtering (GIF) system attached

to the same microscope with an energy resolution of ∼1.0 eV. Note that such an energy resolution is not comparable to that of the X-ray magnetic circular dichroism measurement, and thus the fine features in the corresponding EELS edges are not available. In performing both the ALCHEMI–EELS and EMCD experiments, a convergent beam was used and the EELS data were collected in the diffraction mode. By choosing an appropriate convergent angle (∼2 mrad in the present study) for the incident beam, a small electron probe of adequate intensity can be obtained, resulting in a reasonable dichroic signal in the EMCD measurement. The specimen was oriented in a two-beam condition for both ALCHEMI–EELS and EMCD experiments. In the ALCHEMI–EELS experiment, an orientation parameter $\Delta\theta$ is commonly used to describe the deviation of the angle between the incident beam and the atomic planes from the exact Bragg angle. Our experiments on cobalt- and iron-doped ZnO nanostructures were carried out at room temperature with $\Delta\theta$ varying from ∼−1.8 to ∼1.8 mrad from the two-beam conditions of $\mathbf{g} = (0002)$. The ALCHEMI–EELS spectra ranges were set long enough to include the oxygen K-edge (at 532 eV), cobalt or iron L-edges (at 779 eV and 708 eV, respectively), and the zinc L-edge (at 1,020 eV). The EELS spectra background was subtracted before being processed to generate the normalized peak intensities of zinc, cobalt and iron with respect to that of oxygen. The EMCD measurements were performed with either the objective lens or the Lorentz lens for different measurements. The objective lens exerted a magnetic field of ∼2 T on the specimen, whereas only a very small field (∼17 Oe) applied in the Lorentz lens mode (objective lens off). Use of the Lorentz lens enabled the EMCD measurement to be carried out in the absence of the objective lens without significantly sacrificing measurement spatial resolution[23]. A more detailed description of ALCHEMI–EELS and EMCD methodologies can be found in the Supplementary Information.

References

1. Wolf, S. A. *et al*. Spintronics: a spin-based electronics vision for the future. *Science* **294,** 1488–1495 (2001).
2. Sharma, P. *et al*. Ferromagnetism above room temperature in bulk and transparent thin films of Mn-doped ZnO. *Nature Mater.* **2,** 673–677 (2003).
3. Kittilstved, K. R., Lin, W. K. & Gamelin, D. R. Electronic structure origins of polarity-dependent high-T_C ferromagnetism in oxide-diluted magnetic semiconductors. *Nature Mater.* **5,** 291–297 (2006).
4. Radovanovic, P. V. & Gamelin, D. R. High-temperature ferromagnetism in Ni^{2+}-doped aggregates prepared from colloidal diluted magnetic semiconductor quantum dots. *Phys. Rev. Lett.* **91,** 157202 (2003).
5. Quilty, J. W. *et al*. Signature of carrier-induced ferromagnetism in $Ti_{1-x}Co_xO_{2-\delta}$: exchange interaction between high-spin Co^{2+} and the Ti 3d conduction band. *Phys. Rev. Lett.* **96,** 027202 (2006).
6. Neal, J. R. *et al*. Room-temperature magneto-optics of ferromagnetic transition-metal-doped ZnO thin films. *Phys. Rev. Lett.* **96,** 197208 (2006).
7. Matsukura, F., Ohno, H., Shen, A. & Sugawara, Y. Transport properties and origin of ferromagnetism in (Ga,Mn)As. *Phys. Rev. B.* **57,** R2037–R2040 (1997).
8. Toyosaki, H. *et al*. Anomalous Hall effect governed by electron doping in a room-temperature transparent ferromagnetic semiconductor. *Nature Mater.* **3,** 221–224 (2004).
9. Shinde, S. R. *et al*. Co-occurrence of superparamagnetism and anomalous Hall effect in highly reduced cobalt-doped rutile $TiO_{2-\delta}$ films. *Phys. Rev. Lett.* **92,** 166601 (2004).
10. Xu, Q. Y. *et al*. Room-temperature ferromagnetism in ZnO films due to defects. *Appl. Phys. Lett.* **92,** 082508 (2008).
11. Coey, J. M. D., Venkatesan, M. & Fitzgerald, C. B. Donor impurity band exchange in dilute ferromagnetic oxides. *Nature Mater.* **4,** 173–179 (2005).
12. Venkatesan, M., Fitzgerald, C. B., Lunney, J. G. & Coey, J. M. D. Anisotropic ferromagnetism in substituted zinc oxide. *Phys. Rev. Lett.* **93,** 177206 (2004).
13. Jiang, N. *et al*. Polarity determination by atomic location by channeling-enhanced microanalysis. *Appl. Phys. Lett.* **80,** 389–391 (2001).
14. Kong, X., Hu, G. Q., Duan, X. F., Lu, Y. & Liu, X. L. Polarity determination for GaN thin films by electron energy-loss spectroscopy. *Appl. Phys. Lett.* **81,** 1990–1992 (2002).
15. Liu, Y. Z. *et al*. Co location and valence state determination in ferromagnetic ZnO:Co thin films by atom-location-by-channeling-enhanced-microanalysis electron energy-loss spectroscopy. *Appl. Phys. Lett.* **90,** 154101 (2007).
16. Wang, X. F. *et al*. Signature of intrinsic high-temperature ferromagnetism in cobalt-doped zinc oxide nanocrystals. *Adv. Mater.* **18,** 2476–2480 (2006).
17. Hébert, C. & Schattschneider, P. A proposal for dichroic experiments in the electron microscope. *Ultramicroscopy* **96,** 463–468 (2003).
18. Schattschneider, P. *et al*. Detection of magnetic circular dichroism using a transmission electron microscope. *Nature* **441,** 486–488 (2006).
19. Stöhr, J. Exploring the microscopic origin of magnetic anisotropies with X-ray magnetic circular dichroism (XMCD) spectroscopy. *J. Magn. Magn. Mater.* **200,** 470–497 (1999).
20. Egerton, R. F. *Electron Energy Loss Spectroscopy in the Electron Microscope* 2nd edn (Plenum Press, 1996).
21. Kittel, C. *Introduction to Solid States Physics* 7th edn (Wiley, 1996).
22. Muller, S., Zhou, M. J., Li, Q. & Ronning, C. Intra-shell luminescence of transition-metal-implanted zinc oxide nanowires. *Nanotechnology* **20,** 135704 (2009).
23. Schattschneider, P. *et al*. Magnetic circular dichroism in EELS: Towards 10 nm resolution. *Ultramicroscopy* **108,** 433–438 (2008).

Author contributions

Z.H.Z. and Q.L. conceived and designed the experiments, analysed the data and co-wrote the paper. Z.H.Z. performed the electron microscopy experiments. S.M. contributed iron-doped materials and X.F.W. contributed cobalt-doped ZnO materials. S.M., X.F.W., C.R. and J.B.X. performed the magnetic and optical characterizations on a macroscopic scale and analysed the data. All authors discussed the results and commented on the manuscript.

Additional information

Supplementary information accompanies this paper at www.nature.com/naturenanotechnology. Reprints and permission information is available online at http://npg.nature.com/reprintsandpermissions/. Correspondence and requests for materials should be addressed to Q.L.